Hard X-ray multilayer mirror round-robin on the wavefront preservation capabilities of W/B$_4$C coatings

A. Rack

European Synchrotron Radiation Facility, France

Corresponding author's contact details:

ESRF – S-19, BP 220, F-38043 Grenoble Cedex 9, France

tel: +33 (0)476 88 1781, fax: +33 (0)476 88 2252, e-mail: `arack@snafu.de`

L. Assoufid and W.-K. Lee and B. Shi and C. Liu

Advanced Photon Source, Argonne National Laboratory, USA

Ch. Morawe and R. Kluender

European Synchrotron Radiation Facility, Grenoble, France

R. Conley and N. Bouet

National Synchrotron Light Source II,
Brookhaven National Laboratory, USA

June 23, 2012

Abstract

A round-robin between the multilayer deposition laboratories of the Advanced Photon Source, the European Synchrotron Radiation Facility and the National Synchrotron Light Source II has been initiated in order to study standard W/B_4C multilayer mirrors produced by the different facilities. The use of such multilayer mirrors for hard X-ray monochromatisation represents an important alternative to crystal-based devices when greater photon flux density is desirable for, e. g., X-ray imaging applications and other photon-intensive techniques. Currently, knowledge about the potential degradation of the wavefront in terms of beam profile distortion and coherence properties due to reflection on a multilayer mirror is limited. In order to address this issue, the beam profile and coherence properties of a monochromatic synchrotron beam reflected by the individual mirrors was studied at the Advanced Photon source insertion device beamline 32-ID. The results indicate that by using the same coating material, commercially available high quality substrates and a similar coating technique, mirrors with comparable performance can be produced with quite different multilayer deposition facilities. Furthermore, no wave-optical formalism is available at this time which relates the influence of a multilayer reflection on the wavefront to the structural quality of the mirror. Hence, the experimental studies presented are highly targeted in order to identify parameters which have a potential influence on the wavefront preservation properties of a multilayer.

Keywords: Multilayer mirrors, W/B_4C, Synchrotron radiation, X-rays, Talbot, X-ray phase contrast, X-ray monochromators

1 Introduction

The work presented in this article is part of a larger effort to optimize multilayer mirrors in terms of their influence on the beam profile and coherence properties of a reflected synchrotron beam. Multilayer mirrors are widely deployed as monochromators due to the far higher photon flux possible compared to, for example, Bragg-reflection on a single crystal. However, understanding and mitigating the distortion of the wavefront due to the reflection on such a mirror remains a challenge; striped patterns in the beam profile and significant losses of partial coherence are commonly observed. The availability of a high flux density of coherent photons is crucial for the development and subsequent application of novel imaging techniques such as phase-sensitive tomography (cf., e.g., Nugent (2010)). Increasing coherent photon flux densities with improved X-ray optics such as multilayer mirrors, providing both an increased bandwidth combined with wavefront preservation characteristics competitive to single crystal optics would provide a path to extend the potential impact of existing light sources, without as much of a need for much more cost-intensive machine upgrades.

A recent study revealed that different multilayer compositions seem to have a varying influence on beam profile modification by multilayer-reflection which do not necessarily affect the coherence properties in a negative manner (Rack *et al.* (2010b)). As an outcome of this study, several questions come to bear: reproducibility of the results with mirrors of technically relevant dimensions, influence of processing parameters, substrate quality, buffer and top-coating layers, further material compositions as well as reproducibility with respect to different deposition facilities. It has already been demonstrated that the results are reproducible with respect to the use of different beamlines (see Rack *et al.* (2010b), Rack *et al.* (2012)) as well as being applicable for mirrors of larger dimensions Rack *et al.* (2011).

The question for the reproducibility with respect to different deposition facilities is addressed now in a round-robin of the multilayer laboratories of the Advanced Photon Source (APS), Argonne National Laboratory, USA, the European Synchrotron Radiation Facility (ESRF), Grenoble, France and the National Synchrotron Light Source II (NSLS-2), Brookhaven National Laboratory, USA. The results of a study on the wavefront preservation properties of those samples are

summarised in this article. They are of high interest for synchrotron facilities currently refurbishing or designing new beamlines; frequently, the desired wavefront preservation capabilities of a multilayer mirror are hard to specify as they can depend on numerous parameters. Often, the well established W/B_4C multilayer material system is frequently chosen in lieu of other, perhaps slightly higher performing material systems, because it is so well understood and accepted.

2 Multilayers

There is a tremendous variety of multilayer material systems available (see for example Spiller (1994), Ziegler (1995)). Frequently, the composition chosen depends largely on the photon energy, however at the same time, aspects such as heat load, temporal stability, and environment have to be considered as well. For the study presented within this article, W/B_4C was chosen as W-based multilayers are widely used as monochromators for hard X-ray imaging stations at synchrotron light sources around the globe (ID19 – ESRF, France, see Weitkamp *et al.* (2010), tomcat – Suisse Light Source, Switzerland, see Stampanoni *et al.* (2007), 2-BM – Advanced Photon Source, USA, see Chu *et al.* (2002), BAM*line* – BESSY-II, Germany, see Rack *et al.* (2008), FLUO and TopoTomo – ANKA light source, Germany, see Simon *et al.* (2003); Rack *et al.* (2010a), tomography beamline of CAMD, USA, see Ham *et al.* (2002), beamline 8.3.2 of the Advanced Light Source and 1B2/microprobe of the Pohang Light Source, see Jheon *et al.* (2006)).

For the multilayers produced within this round-robin, both d-spacing and the number of deposited layers were allowed to vary; previous experiments have indicated no measurable influence of the latter on beam profile and coherence properties of the reflected beam (Morawe *et al.* (2011), Rack *et al.* (2010b), Rack *et al.* (2011)). The nominal parameters of the multilayer mirrors are summarized in Tab. 1. Commercial single-side superpolished silicon single crystals produced by the same supplier (General Optics, Gooch & Housego) were used as substrates in all cases to minimize any potential influence of substrate variation on the study.

2.1 APS multilayer fabrication

The APS multilayer was made using magnetron sputtering in a large deposition system with a base pressure of $\sim 1.3 \times 10^{-11}$ bar. A multilayer of 60 bilayers of nominal 1.06 nm W and 1.10 nm B_4C was grown on a super-polished 25 mm $\times$ 50 mm $\times$ 4.5 mm Si substrate (General Optics (USA)) with a nominal 10 nm Cr buffer layer (B_4C is the topmost layer, and W is on the Cr). The growth was carried out under 3.0 µbar of Ar atmosphere using a constant DC power of 150 W for W and 250 W for B_4C. During the deposition, the substrates were translated linearly at constant speeds across a shaped mask over the sputter gun. The distance from the top of the sputter target to the substrate was set to $\sim$12 cm. The layer thicknesses were controlled by the substrate translation speed, with all other deposition parameters fixed. The speeds varied from $\sim$1.5 cm/s to 5 cm/s, which were determined by previous thickness calibrations (Liu *et al.* (2001)).

2.2 ESRF multilayer fabrication

A multilayer coating was made at the ESRF multilayer deposition facility which is based on magnetron sputtering as well (Morawe *et al.* (2007)). The W/B_4C multilayer with a d-spacing of 4.0 nm was deposited in a 1 µbar Ar atmosphere. The filling factor defining the thickness ratio between the W layer and the d-spacing was set to $\Gamma = 0.5$. The applied power was chosen between 50 W for W and 400 W for B_4C in order to obtain comparable sputter rates of 0.1 - 0.2 nm/s. The multilayer was deposited on high quality 100 mm $\times$ 20 mm $\times$ 18 mm Si substrates, again, purchased from General Optics (USA). A 10 nm thick Cr buffer layer was grown on the substrate before the deposition of the multilayer stack. The multilayer deposition started with B_4C and ended with B_4C cap layer.

2.3 NSLS-2 multilayer fabrication

The NSLS-2 multilayer deposition system employs horizontal sputtering from fixed, solid sources through a figured mask onto a sample which is raster scanned across the flux field using a precision linear translation system (Conley *et al.* (2009)). The W/B_4C multilayer (B_4C with 1.05 nm and W with 1.05 nm on 10 nm Cr buffer layer on top of the substrate, B_4C is the topmost layer, and W is on the Cr)

studied was grown as part of the commissioning process for the multilayer Laue lens deposition system. A silicon substrate, also fabricated by General Optics (USA) , with dimensions of 25 mm × 50 mm × 4.5 mm was used. The substrates was raster-scanned horizontally past 75 mm diameter cathodes, for which vertical film uniformity is controlled with the figured masks. Deposition pressure was maintained at 2.7 µbar by injection of approximately 26 standard cubic centimetre of Ar around the dark-space shields. The source to substrate distance was 85 mm. W was deposited at 110 W and 41.5 mm/sec substrate velocity, and B_4C was deposited at 250 W and 9.5 mm/sec substrate velocity. The poor quality of the multilayer grown is caused by a depth-gradient within the stack due to growth rate decay from target erosion. This erosion was intentionally not compensated for during the growth in order to calibrate a substrate velocity-based compensation factor for target erosion for the multilayer Laue lens project.

2.4 X-ray reflectometry

All multilayers were characterized under the same conditions at the ESRF by x-ray reflectometry using a laboratory reflectometer. The reflectometer operates with a IµS [1] 30 W micro-focus Cu tube at 8048 eV, a Montel multilayer collimator, and a Ge(111) monochromator (Incoatec GmbH, Geesthacht (Germany) (2012)). It generates a beam with an angular resolution of about 0.007^o FWHM (full width at half maximum). Specular reflectivity data can be measured with a dynamical range of up to 10^7. The reflectivity scans are shown in Fig. 1. All samples were measured along the center position. Simulation software based on the Parratt formalism (Parratt (1954)) allows for the precise determination of thicknesses t, mass densities ρ, and RMS (root mean square) interface widths σ. In the simulations, the optical densities were assumed to be proportional to the mass densities.

For the APS multilayer, its structure is given as $[B_4C(0.98 \text{ nm})/W(1.20 \text{ nm})]_{60}/Cr(10.6 \text{ nm})/Si$, including a Cr buffer layer. In order to reach a good fit of the simulations to the experimental data the two upper periods of the coating were assumed to be oxidized. The full simulation parameters are shown in Tab. 2.

For the ESRF multilayer, the overall structure of the sample is given by

6

$B_4C/[W/B_4C]_{60}/Cr/Si$, including a Cr buffer and a B_4C cap layer. The corresponding simulation parameters are summarized in the Tab. 3.

The NSLS-2 multilayer shows the following structure $[B_4C(1.32\,\mathrm{nm})/W(0.78\,\mathrm{nm})]_{200}/Cr(10.0\,\mathrm{nm})/Si$, including a Cr buffer layer. Similar to the APS multilayer, the two upper periods of the coating were assumed to be oxidized. The full simulation parameters are listed in Tab. 4.

All three laboratories have produced W/B_4C multilayers with comparable fundamental properties. The essential differences lie within their respective d-spacings and layer numbers. Additional aspects such as surface oxidation and period thickness drift add complications in the data analysis. Therefore, the values shown in Tabs. 2-4 must not be interpreted in the most rigorous manner.

3   Experimental Setup & Data Processing

Experiments were carried out at the insertion device beamline 32-ID of the Advanced Photon Source (Shen *et al.* (2007)). The general layout of the experimental setup used is sketched in Fig. 2: the radiation originating from the undulator insertion device (275 µm × 40 µm (horizontal × vertical, FWHM) effective photon source size) passes through a double-crystal monochromator. An X-ray photon energy of 18 keV is chosen to illuminate a multilayer mirror placed 73 m downstream of the source. In this single-bounce geometry, the beam is vertically reflected by the multilayer and passes a Si phase grating (6 µm pitch) which is located approximately 175 mm downstream (David and Hambach (1999)). The incident angle for each multilayer mirror was set manually to the first respective Bragg peak. The grating is mounted on a sample manipulator in order to translate it out of the beam in order to take reference images. Downstream of the grating, an imaging detector is positioned on a linear stage allowing translation along the beam over a travel range of 655 mm. The detector operates with an effective pixel size of 0.7 µm and a spatial resolving power well below 2 µm – measured using an X-ray test pattern (model X-500-200-30 by Xradia, Pleasanton, CA, USA). Images of the grating and the beam profile are acquired for a selection of different distances between the grating and detector (from 185 mm to 840 mm, 24 steps). A second imaging detector (1.1 µm effective pixel size) placed approximately 3.25 m downstream of the

7

multilayer mirror is employed to record the beam profile for a longer propagation distance. A similar protocol was already successfully deployed at the beamline ID19 of the European Synchrotron Radiation Facility in order to characterize multilayer mirrors (Rack *et al.* (2010b), Rack *et al.* (2011)).

For processing the images of the Si grating, standard darkfield and flatfield corrections are applied first. The horizontal and vertical visibility of the grating structure is then measured in Fourier space, using existing code (Kluender *et al.* (2009)). Plots of the visibility for different grating-detector distances allow for comparing the wavefront preservation capabilities of the different mirrors in a qualitative manner. The ratio of the visibility values for the two Talbot distances given can be used to estimate the effective photon source size which also allows one to characterize the performance of the mirrors in a quantitative manner (Cloetens *et al.* (1997); Kluender *et al.* (2009)).

4 Results

The images showing the profile of the reflected beam captured 3.25 m downstream of the multilayer mirror are presented in Fig. 3. The gray-values for each image were normalized with respect to the mean gray-value. For each profile, a single vertical line profile plot is depicted as well. A vertical intensity gradient is visible for each beam profile, which is most likely related to the intensity profile of the incoming beam. In addition, each beam profile shows the typical stripe pattern which has been observed previously for multilayer reflections (Rack *et al.* (2010b)). The intensity (peak-to-valley) along with the frequency of the stripes is comparable for the three images. We note that there is no significant difference in the profile of the beam after reflection by any of the three multilayer mirrors studied.

The results of the visibility measurements are shown in Fig. 4. Along with the plots for the multilayer mirrors, the visibility plot for the synchrotron beam after transiting only the double-crystal monochromator is also shown. For each plot, the horizontal and vertical effective and angular source sizes are calculated from the two Talbot distances given (Cloetens *et al.* (1997)). For the plot corresponding to the beam without a multilayer reflection, the horizontal effective source size measured matches the theoretical value of 275 µm. The vertical effective source size is not

accessible as the measured visibility of the grating increases with distance. This might be related to beam divergence which can artificially increase the image of the grating structure in the direction of the reflection and hence increase its visibility. Regarding the three plots showing the visibility for the beam reflected by one of the multilayer mirrors, the curve representing the vertical visibility is significantly rougher around the second Talbot distance, suggesting an imperfect flatfield correction due to the stripes caused by the multilayer (cf. Fig. 3). This effect is extremely pronounced for the plot corresponding to the NSLS-II multilayer for distances between 600 mm and 700 mm in both directions. All values for the horizontal source size are similar to the value determined where only the double-crystal monochromator is in the beam. The vertical source size in the direction of the reflection by the multilayer mirrors is significantly altered, enlarged by approximately a factor of three with respect to the theoretical value for all three mirrors.

5   Discussion

The characterization of the wavefront preservation capabilities of three W/B_4C multilayer mirrors for high-energy synchrotron radiation has shown that the beam profile is significantly affected by just a single reflection; stripe patterns in the beam profile are visible, an effect already demonstrated by multilayer mirrors (Rack *et al.* (2010b)). The coherence properties of the synchrotron beam are affected as well, displayed by the significantly enlarged source size in the direction of the reflection. Degradation of the coherence properties due to reflection on a multilayer mirror is known as well (Rack *et al.* (2010b)). The rather strong degradation here compared to multilayers in use as monochromators at other light sources (cf. the BAM*line* at the BESSY-II light source, Germany (Rack *et al.* (2008)), the TopoTomo beamline at the ANKA light source, Germany (Rack *et al.* (2009)) as well as the beamline ID19 of the ESRF (Rack *et al.* (2011))) is most probably related to the rather simple mechanical mount employed (e. g., no cooling of the mirror).

6   Conclusions

The results of the multilayer round-robin presented in this articles allows one to draw several conclusions; first, it is important to note that the influence of the multilayer reflection on the hard synchrotron radiation beam is significant. Here, the findings are agreement with several prior studies Rack *et al.* (2010b), Rack *et al.* (2011), Snigirev (1996), Morawe *et al.* (2011). Second, as also reported in previous studies, the wavefront preservation properties of a coating material combination appear to uninfluenced by d-spacing variations, the number of bi-layers, or substrate dimensions. The round-robin enabled a further study into the coherence-altering properties of multilayer mirrors grown at different laboratories. While the basic coating technique remained the same for all samples, several structural parameters differed between the respective multilayers. Despite these differences, the wavefront preservation properties of the three mirrors studied are very similar. It appears that the characteristic stripe patterns in the beam profile for a given material composition are rather independent of the production environment at the involved laboratories. Our results indicate that other, perhaps substrate-related origins drive the performance of multilayer mirrors in terms of wavefront preservation. A first potential explanation was published by Ziegler *et al.* (1999): the modulation of the beam profile due to reflection on a multilayer mirror is driven by the height error of the mirror surface which introduces a phase distortion. The surface error of the mirror itself is given by the figure error of the substrate which is closely reproduced by the coating. Recently, Morawe *et al.* (2011) published a study using partially coated substrates that supports this hypothesis. The results presented here on the wavefront preservation properties of multilayer mirrors suggest that the following topics of investigation should be initiated: i) a study on how variation of the substrate quality can change the wavefront profile. ii) an investigation into other material compositions and their impact on an the reflected beam profile and wavefront coherence properties, cf. Rack *et al.* (2010b).

Acknowledgments

References

Chu, Y. S., Liu, C., Mancini, D. C., De Carlo, F., Macrander, A. T., Lai, B., and Shu, D. 2002. Performance of a double-multilayer monochromator at beamline 2-bm at the advanced photon source. Rev. Sci. Instrum. 73, 1485–1487.

Cloetens, P., Guigay, J. P., De Martino, C., Baruchel, J., and Schlenker, M. 1997. Fractional talbot imaging of phase gratings with hard x rays. Opt. Lett. 22, 1059–1061.

Conley, R., Bouet, N., Biancarosa, J., Shen, Q., Boas, L., Feraca, J., and Rosenbaum, L. 2009. The nsls-ii multilayer laue lens deposition system. In: Advances in X-Ray/EUV Optics and Components IV (*eds.* A. M. Khounsary, C. Morawe, and S. Goto), p. 74480U, volume 7448 of *Proc. of SPIE*, p. 74480U.

David, C. and Hambach, D. 1999. Line width control using a defocused low voltage electron beam. Microelectron. Eng. 46, 219–222.

Ham, K., Jin, H., Butler, L. G., and Kurtz, R. L. 2002. A microtomography beamline at the louisiana state university center for advanced microstructures and devices synchrotron. Rev. Sci. Instrum. 73, 1521–1523.

Incoatec GmbH, Geesthacht (Germany) 2012. Iμs source. http://www.incoatec.de.

Jheon, S., Youn, H.-S., Kim, H.-T., Choi, G.-H., and Kim, J.-K. 2006. High-resolution x-ray refraction imaging of rat lung and histological correlations. Microsc. Res. & Tech 69, 656–659.

Kluender, R., Masiello, F., van Vaerenbergh, P., and Härtwig, J. 2009. Measurement of the spatial coherence of synchrotron beams using the talbot effect. Phys. Status Solidi A 206, 1842–1845.

Liu, C., Macrander, A., Als-Nielsen, J., and Zhang, K. 2001. Laterally graded multilayers and their applications. J. Vac. Sci. Technol. A 19, 1421–1424.

Morawe, C., Barrett, R., Friedrich, K., Klünder, R., and Vivo, A. 2011. Spatial coherence studies on x-ray multilayers. In: Advances in X-Ray/EUV Optics and Components VI (*eds.* C. Morawe, A. M. Khounsary, and S. Goto), p. 813909, volume 8139 of *Proc. of SPIE*, p. 813909.

Morawe, C., Borel, C., and Peffen, J.-C. 2007. The new esrf multilayer deposition facility. In: Advances in X-Ray/EUV Optics and Components II (*eds.* A. M. Khounsary, C. Morawe, and S. Goto), p. 670504, volume 6705 of *Proc. of SPIE*, p. 670504.

Nugent, K. A. 2010. Coherent methods in the x-ray sciences. Adv. Phys. 59, 1–99.

Parratt, L. A. 1954. Surface studies of solids by total reflection of x-rays. Phys. Rev. 45, 359–369.

Rack, A., Assoufid, L., Dietsch, R., Weitkamp, T., Trabelsi, S. B., Rack, T., Siewert, F., Krämer, M., Holz, T., Zanette, I., Lee, W.-K., Cloetens, P., and Ziegler, E. 2012. Study of multilayer-reflected beam profiles and their coherence properties using beamlines id19 (esrf) and 32-id (aps). In: AIP Conference Proceedings (ICXOM21) (*eds.* C. A. Pérez and A. M. de Souza), pp. 15–17, volume 1437, pp. 15–17.

Rack, A., Riesemeier, H., Vagovič, P., Weitkamp, T., Siewert, F., Dietsch, R., Diete, W., Bauer Trabelsi, S., Waterstradt, T., and Baumbach, T. 2010a. Fully automated, fixed exit, in vacuum double-multilayer monochromator for synchrotron-based hard x-ray micro imaging applications. volume 1234 of *AIP Conf. Proc. (SRI09)*, pp. 734–737.

Rack, A., Weitkamp, T., Bauer Trabelsi, S., Modregger, P., Cecilia, A., dos Santos Rolo, T., Rack, T., Haas, D., Simon, R., Heldele, R., Schulz, M., Mayzel, B., Danilewsky, A. N., Waterstradt, T., Diete, W., Riesemeier, H., Müller, B. R., and Baumbach, T. 2009. The micro-imaging station of the topotomo beamline at the anka synchrotron light source. Nucl. Instr. & Meth. in Phys. Res. B 267, 1978–1988.

Rack, A., Weitkamp, T., Riotte, M., Grigoriev, D., Rack, T., Helfen, L., Baumbach, T., Dietsch, R., Holz, T., Krämer, M., Siewert, F., Meduňa, M., Cloetens, P., and Ziegler, E. 2010b. Comparative study of multilayers used in monochromators for synchrotron-based coherent hard x-ray imaging. J. Synchrotron Radiat. 17, 496–510.

Rack, A., Weitkamp, T., Zanette, I., Morawe, C., Rommeveaux, A. V., Tafforeau, P., Cloetens, P., Ziegler, E., Rack, T., Cecilia, A., Vagovic, P., Harmann, E., Dietsch, R., and Riesemeier, H. 2011. Coherence preservation and beam flatness of a single-bounce multilayer monochromator (beamline id19–esrf). Nucl. Instrum. & Meth. in Phys. Res. A 649, 123–127. Proc. of the 15th National Conference on Synchrotron Radiation Research – SRI 2010.

Rack, A., Zabler, S., Müller, B., Riesemeier, H., Weidemann, G., Lange, A., Goebbels, J., Hentschel, M., and Görner, W. 2008. High resolution synchrotron-based radiography and tomography using hard x-rays at the bamline (bessy ii). Nucl. Instrum. & Meth. in Phys. Res. A 586, 327–344.

Shen, Q., Lee, W.-K., Fezzaa, K., Chu, Y. S., Carlo, F. D., Jemian, P., Ilavsky, J., Erdmann, M., and Long, G. G. 2007. Dedicated full-field x-ray imaging beamline at advanced photon source. Nucl. Instrum. & Meth. in Phys. Res. A 582, 77–79. Proc. of the 14th National Conference on Synchrotron Radiation Research – SRI 2007.

Simon, R., Buth, G., and Hagelstein, M. 2003. The x-ray-fluorescence facility at anka, karlsruhe: Minimum detection limits and micro probe capabilities. Nucl. Instrum. & Meth. in Phys. Res. B 199, 554–558.

Snigirev, A. A. 1996. Coherent properties of the third-generation synchrotron radi-

ation sources: optical requirements. In: Optics for High-Brightness Synchrotron Radiation Beamlines II (*eds.* L. E. Berman and J. Arthur), pp. 26–33, volume 2856 of *Proc. of SPIE*, pp. 26–33.

Spiller, E. 1994. Soft X-Ray Optics. SPIE Press, Bellingham, WA.

Stampanoni, M., Groso, A., Isenegger, A., Mikuljan, G., Chen, Q., Meister, D., Lange, M., Betemps, R., Henein, S., and Abela, R. 2007. Tomcat: A beamline for tomographic microscopy and coherent radiology experiments. In: AIP Conference Proceedings (SRI2006) (*eds.* J.-Y. Choi and S. Rah), pp. 848–851, volume 879, pp. 848–851.

Weitkamp, T., Tafforeau, P., Boller, E., Cloetens, P., Valade, J.-P., Bernard, P., Peyrin, F., Ludwig, W., Helfen, L., and Baruchel, J. 2010. Status and evolution of the esrf beamline id19. volume 1221 of *AIP Conf. Proc. (ICXOM20)*, pp. 33–38.

Ziegler, E. 1995. Multilayers for high heat load synchrotron applications. Opt. Eng. 34, 445–452.

Ziegler, E., Morawe, C., Hignette, O., Cloetens, P., and Tucoulou, R. 1999. Multilayer x-ray optics for high energy third-generation synchrotron sources: the state of the art. In: Ninth International Conference on Production Engineering, Precision Science and Technology for Perfect Surfaces (*eds.* Y. Furukawa, Y. Mori, and T. Kataoka), pp. 285–291, volume 3 of *Japan Society for Precision Engineering Proc.*, pp. 285–291.

A   Figures
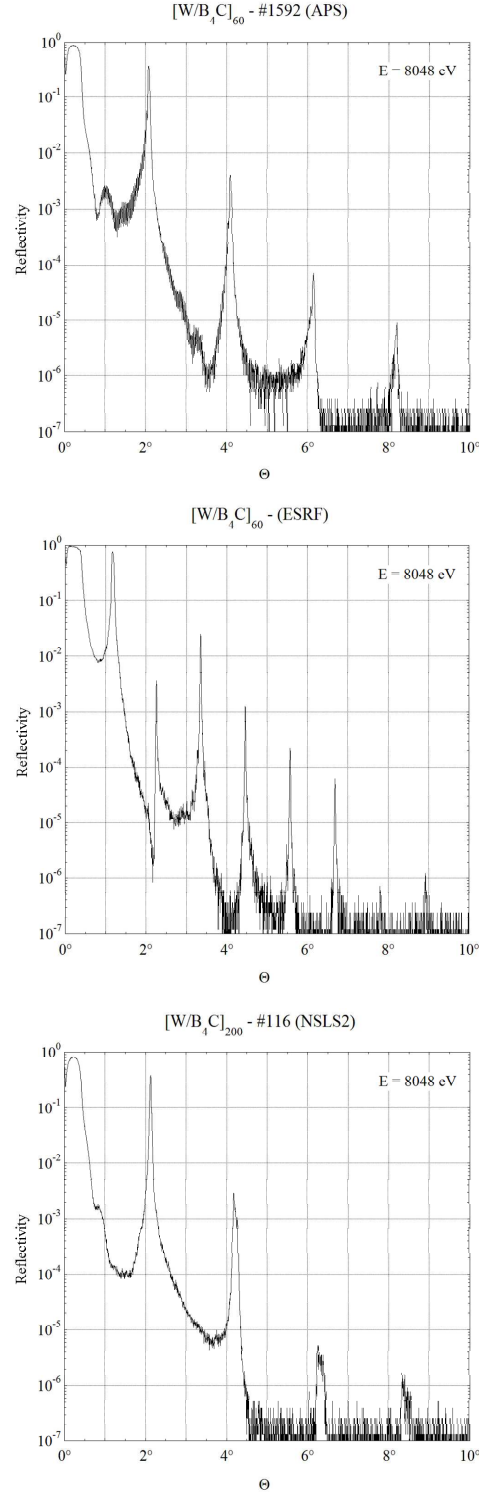
Figure 1:   (1-column-span) X-ray reflectivity scans of the three multilayers studied (Cu kα radiation). Parameters of simulated reflectivity curves fitted to the experimental data are summarized in Tabs. 2, 3 and 4.
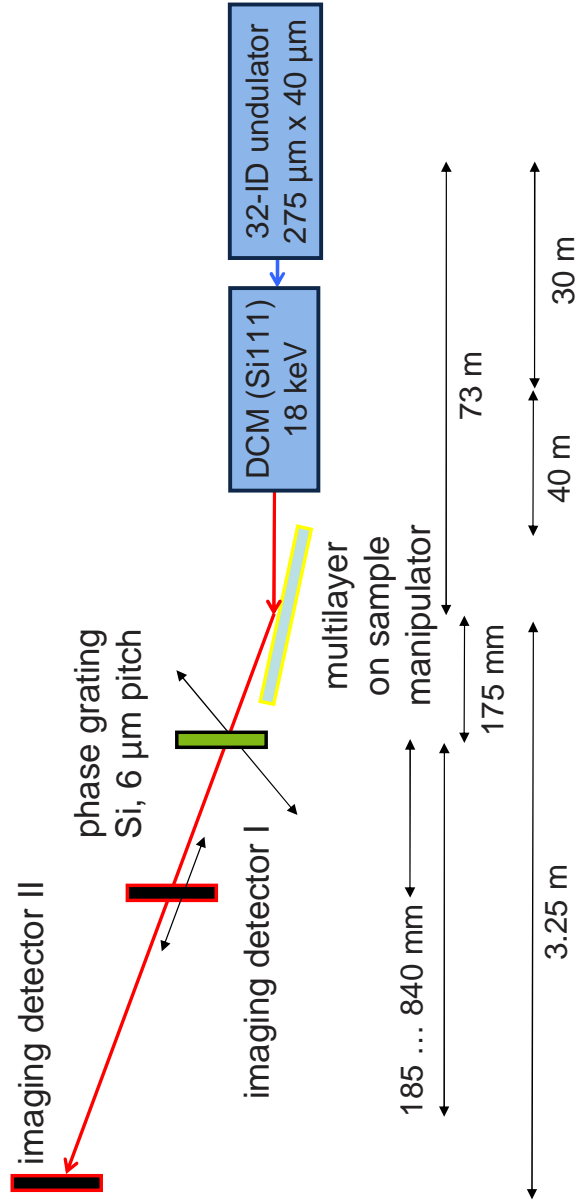
15

Figure 2: (Color online, rotate 90 degree, 1.5-column-span) Sketch of the experimental setup realised at the APS beamline 32-ID-C for the characterization of the wavefront preservation capabilities of the multilayer mirrors: the radiation from an undulator insertion device (275 µm × 40 µm (horizontal × vertical, FWHM) effective photon source size) after passing a crystal monochromator (18 keV) is vertically reflected by one of the multilayer mirrors (Shen *et al.* (2007)). The beam passes a Si phase grating (6 µm pitch), at different distances between the grating and the 'imaging detector I' the visibility of the structure within the captured X-ray images is measured. Approximately 3.25 m downstream of the multilayer mirror the profile of the reflected beam is recorded with the 'imaging detector II'.
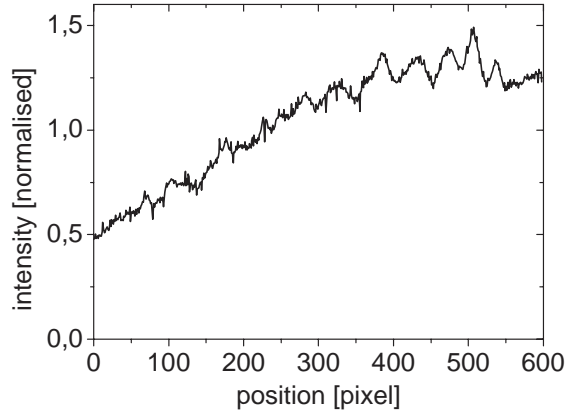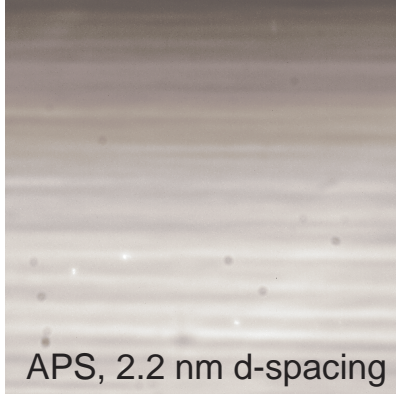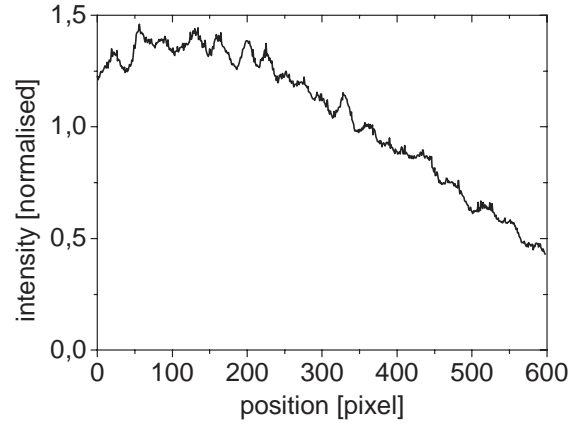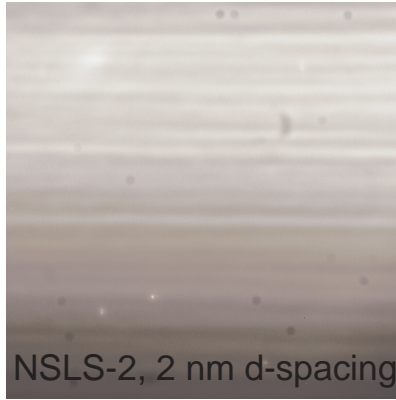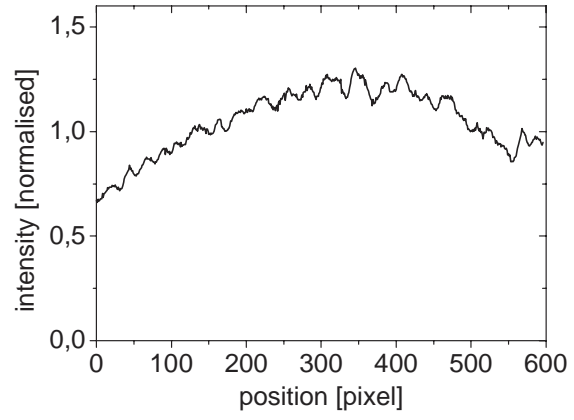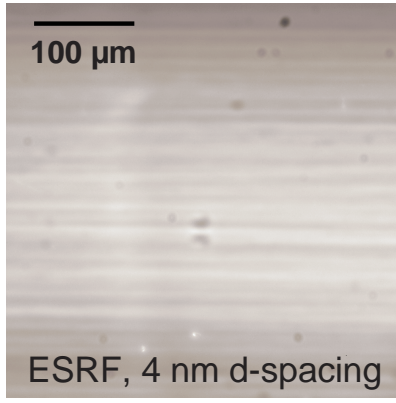
Figure 3: (2-column-span) The profiles of the hard synchrotron beam reflected by the multilayer mirrors under study, after approximately 3.25 m propagation distance (left). Exemplary vertical profile plots are shown on the right side for each reflected beam.
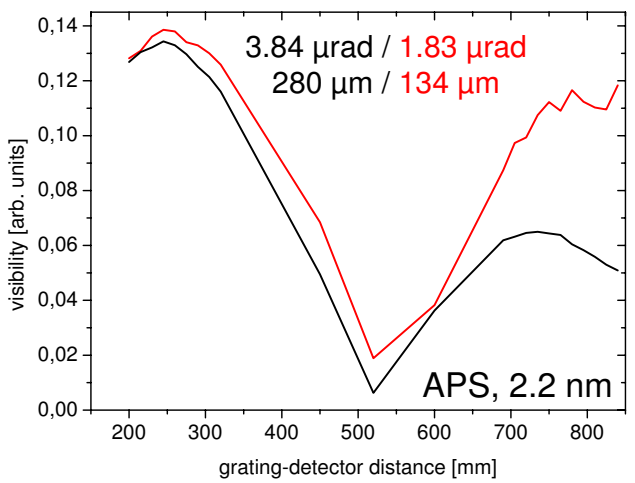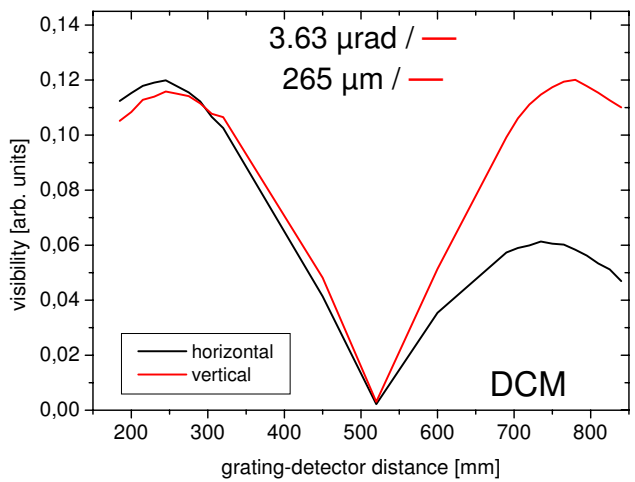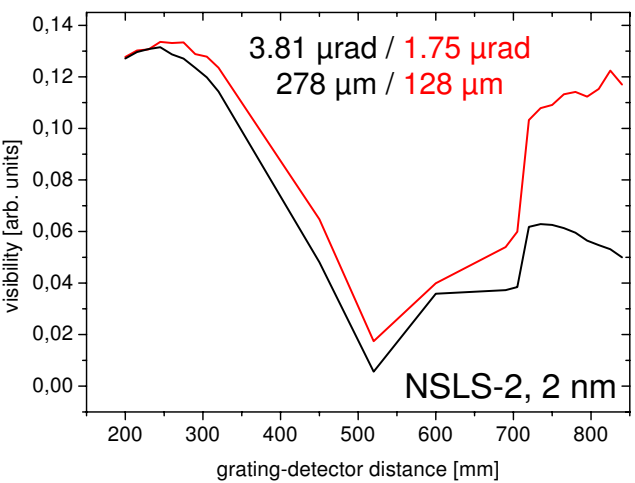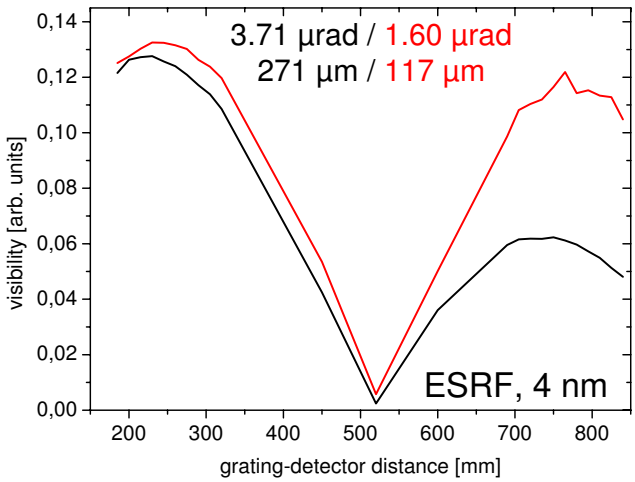
Figure 4: (Color online, rotate 90 degree, 2-column-span) Horizontal as well as vertical visibility of the phase grating for different grating-detector distances. Plots are shown for each multilayer mirror under study as well as for the beam after passing only the double-crystal monochromator. Horizontal and vertical source sizes shown as inset are calculated based on the visibility at the two Talbot distances given (Cloetens *et al.* (1997)).

18

B Tables

facility	d-spacing [nm]	number of bilayers	substrate dimension [mm × mm × mm]
APS	2.2	60	$25 \times 50 \times 4.5$
ESRF	4.0	60	$20 \times 100 \times 18$
NSLS-2	2.0	200	$25 \times 50 \times 4.5$

Table 1: List of the W/B_4C multilayer mirrors studied and their nominal specifications.

layer material	t [nm]	ρ [g/cm^3]	σ [nm]
B_4C (cap layer)	–	–	–
B_4C (periodic)	0.98	2.50	0.20
W (periodic)	1.20	18.5	0.31
Cr (buffer layer)	10.65	7.19	0.20

Table 2: Characteristics of the APS multilayer derived by fitting simulations to the X-ray reflectometry data (t: thickness, ρ mass densities, and RMS interface widths σ).

layer material	t [nm]	ρ [g/cm^3]	σ [nm]
B_4C (cap layer)	2.87	2.40	0.33
W (periodic)	2.11	17.30	0.24
B_4C (periodic)	1.87	2.40	0.30
Cr (buffer layer)	9.90	7.19	0.45

Table 3: Characteristics of the ESRF multilayer derived by fitting simulations to the X-ray reflectometry data.

layer material	t [nm]	ρ [g/cm^3]	σ [nm]
B_4C (cap layer)	–	–	–
B_4C (periodic)	1.32	5.00	0.26
W (periodic)	0.78	17.00	0.26
Cr (buffer layer)	10.00	7.19	0.40

Table 4: Characteristics of the NSLS-2 multilayer derived by fitting simulations to the X-ray reflectometry data.